Environmental Research 211 (2022) 113057

Contents lists available at ScienceDirect

Environmental Research

journal homepage: www.elsevier.com/locate/envres

Effect of electrolyte composition on electrochemical oxidation: Active sulfate formation, benzotriazole degradation, and chlorinated by-products distribution

Pradip Saha [a,b,*], Jiamin Wang [a], Yinong Zhou [a], Livio Carlucci [a], Adriaan W. Jeremiasse [c], Huub H.M. Rijnaarts [a], Harry Bruning [a]

[a] Department of Environmental Technology, Wageningen University and Research, P.O. Box 17, 6700, AA Wageningen, the Netherlands
[b] Department of Chemical Engineering and Polymer Science, Shahjalal University of Science and Technology, Sylhet, 3114, Bangladesh
[c] MAGNETO Special Anodes B.V. (an Evoqua Brand), Calandstraat 109, 3125, BA Schiedam, the Netherlands

ARTICLE INFO

Keywords:
Sulfate radical
Hydroxyl radical
Active chlorine species
Chlorinated transformation products
Boron-doped diamond anode
Benzotriazole

ABSTRACT

Electrochemical oxidation is an effective technique for treating persistent organic pollutants, which are hardly removed in conventional wastewater treatment plants. Sulfate and chloride salts commonly used and present in natural wastewater influence the electrochemical degradation process. In this study, the effect of electrolyte composition on the active sulfate species ($SO_4^{\bullet-}$ and $S_2O_8^{2-}$) formation, benzotriazole degradation-a model organic compound, and chlorinated by-products distribution have been investigated while using a boron-doped diamond (BDD) anode. Different Na_2SO_4:$NaNO_3$ and Na_2SO_4:NaCl ratios with constant conductivity of 10 mS/cm were used in the experiments and applied anode potential was kept constant at 4.3 V vs. Ag/AgCl. The electrogenerated $SO_4^{\bullet-}$ and $S_2O_8^{2-}$ formation were faster in 10:1 and 2:1 Na_2SO_4:$NaNO_3$ ratios than in the 1:0 ratio. The $^{\bullet}$OH-mediated $SO_4^{\bullet-}$ production has prevailed in 10:1 and 2:1 ratios. However, $^{\bullet}$OH-mediated $SO_4^{\bullet-}$ production has hindered the 1:0 ratio due to excess chemisorption of SO_4^{2-} on the BDD anode. Similarly, the faster benzotriazole degradation, mineralization, and lowest energy consumption were achieved in the 10:1 Na_2SO_4:$NaNO_3$ and Na_2SO_4:NaCl ratio. Besides, chlorinated organic by-product concentration (AOX) was lower in the 10:1 Na_2SO_4:NaCl ratio but increased with the increasing chloride ratio in the electrolyte. LC-MS analysis shows that several chlorinated organic transformation products were produced in 0:1 to 2:1 ratio, which was not found in the 10:1 Na_2SO_4:NaCl ratio. A comparatively higher amount of ClO_4^- was formed in the 10:1 ratio than in 2:1 to 0:1 ratio. This ClO_4^- formation train evidence the effective $^{\bullet}$OH generation in a sulfate-enriched condition because the ClO_4^- formation is positively correlated to $^{\bullet}$OH concentration. Overall results show that sulfate-enriched electrolyte compositions are beneficial for electrochemical oxidation of biorecalcitrant organic pollutants.

1. Introduction

In the past few decades, an increasing number of persistent organic pollutants (POPs) have been detected in the aquatic environment due to the rising anthropogenic activities and excessive population growth (Stefan, 2017). Some of those pollutants have shown resistance to conventional biological wastewater treatment processes and enter the aquatic environments through effluents and sludges of wastewater treatment plants, causing threats to the ecosystem and human health (Seibert et al., 2020). Thus, appropriate technology needs to be developed to remove and degrade these bio recalcitrant organic pollutants.

Over the last decade, electrochemical oxidation (EO) with boron-doped diamond (BDD) anode has been considered an attractive technology for the removal of POPs from water because of its high removal efficiency, moderate operating conditions, in-situ oxidant generation, and automatability (Martinez-Huitle et al., 2015; Panizza and Cerisola, 2009). The EO process, with BDD anode, can produce in-situ hydroxyl radicals ($^{\bullet}$OH), reactive sulfate and chloride species from their corresponding salts, which are potent to degrade and mineralize POPs

* Corresponding author. Department of Environmental Technology, Wageningen University and Research, P.O. Box 17, 6700, AA Wageningen, the Netherlands.
E-mail addresses: pradip.saha@wur.nl, pradip-cep@sust.edu (P. Saha).

https://doi.org/10.1016/j.envres.2022.113057
Received 24 August 2021; Received in revised form 24 February 2022; Accepted 27 February 2022
Available online 7 March 2022

including pharmaceuticals, pesticides, plasticizers, dyes, industrial and municipal contaminants (Clematis and Panizza, 2021; dos Santos et al., 2021; Hu et al., 2021; Salazar-Banda et al., 2021; Yang, 2020). Those reactive species were demonstrated faster degradation of the pollutants close to the anode and/or in the bulk solution (Brillas, 2021; Lan et al., 2017).

Sulfate (SO_4^{2-}) is extensively used as support electrolytes in EO experiments and is present in natural and wastewaters. In sulfate-containing electrolytes, sulfate radicals ($SO_4^{\bullet-}$) and peroxydisulfate ($S_2O_8^{2-}$) can be electrochemically generated with the BDD anode (Farhat et al., 2015; Zhang et al., 2015; Thiam et al., 2018). Several studies show that $SO_4^{\bullet-}$ and $S_2O_8^{2-}$ can significantly boost POPs' degradation (Farhat et al., 2015; Shin et al., 2019; Bruguera-Casamada et al., 2016; Villegas-Guzman et al., 2017). Three $SO_4^{\bullet-}/S_2O_8^{2-}$ formation pathways have been reported in the literature, as illustrated in Fig. 1 (Farhat et al., 2015; Zhang et al., 2015; Thiam et al., 2018; Shin et al., 2019; Chen et al., 2018; Davis et al., 2014; Serrano et al., 2002; Ganiyu et al., 2021).

The relevant reactions of the pathways are described below:

$$2SO_4^{2-} \rightarrow S_2O_8^{2-} + 2e^- \quad \text{(Eq. 1)}$$

$$S_2O_8^{2-} \leftrightarrow 2SO_4^{\bullet-} \quad \text{(Eq. 2)}$$

$$SO_4^{2-} \rightarrow SO_4^{\bullet-} + e^- \quad \text{(Eq. 3)}$$

$$SO_4^{2-} + \bullet OH \rightarrow SO_4^{\bullet-} + OH^- \quad \text{(Eq. 4)}$$

$$HSO_4^- + \bullet OH \rightarrow SO_4^{\bullet-} + H_2O \quad \text{(Eq. 5)}$$

$$H_2SO_4 + \bullet OH \rightarrow SO_4^{\bullet-} + H_3O^+ \quad \text{(Eq. 6)}$$

In pathway (a), SO_4^{2-} is directly oxidized to $S_2O_8^{2-}$ on the anode surface (Eq. (1)), which is radically or non-radically activated to $SO_4^{\bullet-}$ (Eq. (2)) (Serrano et al., 2002; Santos et al., 2018; Groenen Serrano, 2018; Araújo et al., 2018). In this way, the increase of SO_4^{2-} concentration would improve the generation of $S_2O_8^{2-}$. In pathway (b), SO_4^{2-} is directly oxidized to $SO_4^{\bullet-}$ by a one-electron transfer reaction (Eq. (3)) (Farhat et al., 2017). Excessive SO_4^{2-} will facilitate more $SO_4^{\bullet-}$ formation, which is further transferred to $S_2O_8^{2-}$ according to a recombination reaction (the reverse reaction of Eq. (2)) (Bagastyo et al., 2020). In pathway (c), $^{\bullet}OH$, generated from water oxidation, mediated electrolysis of SO_4^{2-} to $SO_4^{\bullet-}$, which subsequently is converted to $S_2O_8^{2-}$ (Eqs. (4)–(6)) (Lan et al., 2017; Groenen Serrano, 2018; Farhat et al., 2017; Devi et al., 2013; Ma et al., 2017, 2021). Studies show that a large proportion of $SO_4^{\bullet-}$ was generated by pathway (c) because $^{\bullet}OH$ had a higher oxidative ability, which could also react with HSO_4^- and H_2SO_4 (Chen et al., 2018; Araújo et al., 2018). Thus, it could be hypothesized

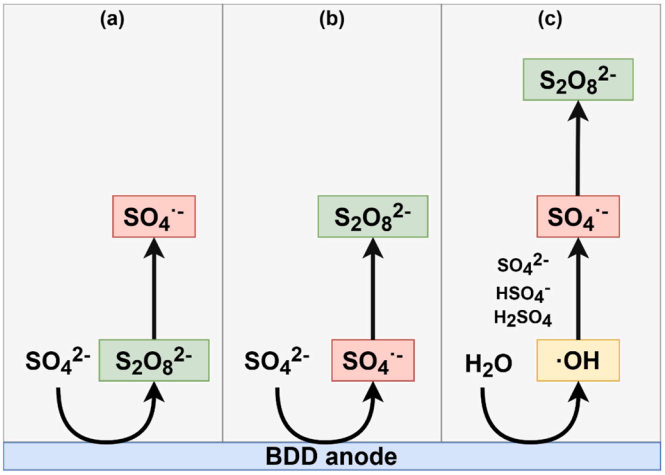

Fig. 1. Possible mechanisms of peroxydisulfate formation with BDD anode.

that the $SO_4^{\bullet-}$ formation rate is related to $^{\bullet}OH$ formation, and an increasing number of $^{\bullet}OH$ will facilitate more $SO_4^{\bullet-}$ and $S_2O_8^{2-}$ formation via the pathway (c).

The SO_4^{2-} concentration influenced the competitive $^{\bullet}OH$ and $S_2O_8^{2-}$ formation reactions (da Costa et al., 2019). At high SO_4^{2-} concentration, two slopes were found in the linear sweep curves corresponding to the transformation of SO_4^{2-} to $S_2O_8^{2-}$ and $^{\bullet}OH$ formation on the electrode surface (Zhang et al., 2015; da Costa et al., 2019). Surface-mediated oxidation of SO_4^{2-} was responsible for $S_2O_8^{2-}$ formation at concentrated SO_4^{2-} electrolytes (Santos et al., 2020). However, the impact of electrolyte composition on $SO_4^{\bullet-}$ formation pathways is still unclear and needs more illustration to maximize the active oxidants formation.

The ubiquitous presence of chloride (Cl^-), which concentration varies from around 0.5 g/L in ground/surface water to 30 g/L in industrial or municipal wastewater discharge. Thus, Cl^- is also commonly studied in the EO process, among other salts. Cl^- is primarily oxidized directly and via $^{\bullet}OH$ on the BDD surface to active chlorine species (Cl_2, ClO^-/HClO) and chlorine radicals ($Cl^{\bullet}$, $Cl_2^{\bullet-}$, $ClOH^{\bullet-}$) (Wang et al., 2020). In many cases, Cl^- presence boosts the organic compound degradation rate due to these reactive species. On the contrary, Cl^- itself will negatively affect the degradation rate of the organic compound. At high Cl^- concentration, $^{\bullet}OH$ is scavenged, and chlorine radicals are formed. Chlorine radicals subsequently convert to dichloride radical ions causing an inefficient oxidation process (Grebel et al., 2010). In the complex transformation process, the formation of active chlorine species and chlorine radicals are considered as the crucial intermediate for the chlorinated by-product formation, including chlorinated organic transformation products (COTPs), chlorate, and perchlorate (Lan et al., 2017). Those by-products often have toxic effects when discharged into the natural aquatic environment.

Moreover, several $SO_4^{\bullet-}$ based advanced oxidation process studies have shown that Cl^- reacts with $SO_4^{\bullet-}$ to form chlorine radicals, which subsequently would participate in the COTPs formation reactions. An $SO_4^{\bullet-}$ base oxidation study showed that the low concentration of Cl^- (1 and 10 mM) increased the degradation rate of benzotriazole. In comparison, a higher concentration of Cl^- (100 mM) decreased the degradation rate because of $SO_4^{\bullet-}$ scavenging by Cl^- (Ma et al., 2021). Thus, the Cl^- concentration in the electrolyte needs to be controlled and regulated to achieve the best degradation performance and stop or minimize the toxic COTPs formation.

EO's large-scale application is still limited because of mass transfer-controlled reaction kinetics, high energy consumption, and chlorinated by-product formation. Membrane separation, including reverse osmosis (RO) and nanofiltration (NF), becomes a promising pre-treatment before EO. Membrane separation increases organic compounds and salts' concentration in concentrate, reducing the transfer limitations and lowering the energy consumption. However, increasing salts concentration also increases the Cl^- concentration, ultimately facilitating undesired chlorinated by-product formation. Recently, research shows that nanofiltration can selectively reject SO_4^{2-} at a higher rate than Cl^- so that the concentrate would be rich in SO_4^{2-} and low in Cl^- (Jin et al., 2020). Thus, integrating EO with nanofiltration may tune the SO_4^{2-} and Cl^- ratio, thereby altering the treatment performance. For instance, EO of bisphenol A in 0.008 M NaCl+0.047 M Na_2SO_4 solution shows better degradation and mineralization than 0.070 M NaCl+0.050 M Na_2SO_4. Also, excess SO_4^{2-} in the electrolyte subsides COTPs formation (Burgos-Castillo et al., 2018). However, the appropriate explanation of this better degradation rate and mineralization still needs further research on whether an optimum electrolyte composition will benefit the degradation rate and reduce the toxic by-product formation.

Therefore, this study elucidates the effect of electrolytes composition, in terms of Na_2SO_4:$NaNO_3$ (SN) ratio at constant conductivity, on electrogenerated $SO_4^{\bullet-}$ and $S_2O_8^{2-}$ formation with boron-doped diamond (BDD) anode. $NaNO_3$ is used in the experiments because $NaNO_3$ is considered inert during electrochemical oxidation (Bruninghoff et al., 2019) and would cause negligible interference in the $S_2O_8^{2-}$ detection

(Gokulakrishnan et al., 2016). Benzotriazole is chosen as a model organic biorecalcitrant pollutant often found in industrial and other wastewater effluents. The influence of Na_2SO_4:$NaNO_3$ (SN) and Na_2SO_4:NaCl (SCl) ratios on benzotriazole degradation kinetics, mineralization efficiency, and energy consumption are reported. The influence of SCl ratio on chlorinated organic transformation product (COTPs) as AOX, chlorate and perchlorate formation are also monitored. Finally, the effect of SCl ratios on possible COTPs distribution has been analyzed by LC-MS. Based on experimental results and existing literature, the reaction mechanisms are discussed.

2. Materials and methods

2.1. Chemicals

Benzotriazole ($C_6H_5N_3$, ≥96%) and sulfuric acid (H_2SO_4, ≥95.0%) were purchased from Sigma Aldrich Chemie BV (the Netherlands). Sodium chloride (NaCl, ≥99.0%), sodium sulfate (Na_2SO_4, ≥99.0%), sodium nitrate ($NaNO_3$, ≥99.0%), sodium peroxydisulfate ($Na_2S_2O_8$, ≥99.0%), disodium hydrogen phosphate dihydrate ($Na_2HPO_4{\cdot}2H_2O$, ≥99.0%), monosodium phosphate dihydrate ($NaH_2PO_4{\cdot}2H_2O$, ≥99.0%), and N, N-diethyl-p-phenylenediamine (DPD) was purchased from VWR chemicals (Leuven Belgium). Milli-Q™ water was used to prepare and dilute all samples unless otherwise stated.

2.2. Experimental set-up

All experiments were conducted in the Environmental technology lab at Wageningen University, the Netherlands. Experiments were performed in an undivided flat cell with an effective projected electrode surface area of 22.4 cm^2, described elsewhere (Saha et al., 2020a). A BDD electrode was employed as the anode, and a platinum-coated titanium electrode was used as the cathode (Magneto Special Anodes, the Netherlands). The distance between the electrodes was 1.5 cm. A silver/silver chloride (Ag/AgCl) electrode connected with Haber Lugging capillaries filled with 10% (W/V) potassium nitrate solution was employed as reference (QM711X/Gel, Prosense, The Netherlands). An IviumStat.h potentiostat with Iviumstat software (Ivium Technologies B. V, the Netherlands) was used to control the voltage and record the experimental data.

2.3. Experimental method

The experiment aimed to elucidate the electrolyte composition impact on dominating active sulfate species formation pathways and benzotriazole degradation rate. The cell was continuously circulated without or with a 10 mg/L benzotriazole solution with different SCl and SN electrolyte ratios at a 580 mL/min flow rate from a 350 mL recirculation bottle. The OLI Studio 9.6 software was used to calculate the amount of salts required to keep the conductivity of the electrolyte at 10 mS/cm (Table 1). 4.3 V vs. Ag/AgCl voltage was applied on the BDD anode. Samples were collected at given time intervals for benzotriazole analysis. Samples were also taken for quantification of total organic carbon (TOC), anions (Cl^-, ClO_3^-, ClO_4^-), free chlorine, COTPs as AOX (adsorbable organic halides), and for the identification of COTPs.

Table 1
Electrolyte composition with 10 (±0.1) mS/cm constant conductivity.

	Ratio	Na_2SO_4 (M)	NaCl (M)	$NaNO_3$ (M)
Na_2SO_4:$NaNO_3$ (SN)	1:0	0.064	–	0
	10:1	0.06	–	0.006
	2:3	0.034	–	0.051
	0:1	0	–	0.1
Na_2SO_4:NaCl (SCl)	1:0	0.064	0	–
	10:1	0.06	0.006	–
	2:1	0.060048	0.024	–
	2:3	0.032	0.047	–
	0:1	0	0.095	–

2.4. Analytical methods

Benzotriazole concentration was analyzed by high-performance liquid chromatography (HPLC, Thermo Scientific) connected with a fluorescence detector with a wavelength set to 278 nm. An ACQUITY UPLC CSH Phenyl-Hexyl column (1.7 μm, 2.1 × 150 mm) was used and kept at a constant temperature of 35 °C. The eluents (A 0.1% formic acid in Milli-Q water and B 0.1% formic acid in acetonitrile) were pumped with a constant flow rate of 0.2 mL/min. The injected volume was 50.00 μL. The instruments were controlled by Chromeleon 6.8. A TOC-$L_{CPH/CPN}$ analyzer connected with an ASI-L autosampler (Shimadzu Corporation (Kyoto, Japan)) was used for TOC measurements. The sample was first acidified by mean of H_2SO_4 to remove all inorganic carbon; the solution was then introduced in a compartment where the organic carbon was oxidized to CO_2 at 720 °C, and last detected by mean of non-dispersive infrared detection. Anions (Cl^-, ClO_3^-, ClO_4^-) concentration was measured by ion chromatography (IC) on Dionex ICS-2100 (Dionex, Breda, The Netherlands), equipped with a Dionex IonPac AS19 column model (4 × 250 mm). Free chlorine concentrations were measured with Hach chlorine DPD test reagent (USEPA-DPD 330.5 method) and a Hach DR/3900 spectrophotometer (Hach Lange GmbH, Düsseldorf, Germany). According to the instructions on the kit test, the Hach LCK390 cuvette and Hach DR/3900 spectrophotometer were used to analyze the AOX concentrations (Hach Lange GmbH, Düsseldorf, Germany). Peroxydisulfate ($S_2O_8^{2-}$) concentration was measured by the DPD-spectrophotometric method described in Gokulakrishnan, Mohammed and Prakash (Gokulakrishnan et al., 2016). 1 mL sample, 5 mL (50 mM) phosphate buffer, 0.1 mL (2.5 mM) DPD solutions, and 3.9 mL Milli-Q water were mixed and incubated for 10 min at room temperature. After that, the mixed solution's absorption spectra were measured at 510 nm and 551 nm by Hach DR/3900 spectrophotometer. Detailed of the TOC, anions, free chlorine, and peroxydisulfate determination methods were reported elsewhere (Saha et al., 2021).

The chlorinated organic transformation products (COTPs) were identified by liquid chromatography combined with high-resolution-accurate-mass mass spectrometry detection (LC-HRAM-MS). The UHPLC Dionex Ultimate 3000 was equipped with an auto-sampler and a temperature-controlled oven compartment coupled with the orbitrap mass spectrometer Q-Executive (Thermo Fisher Scientific, US). After injection of 50 μL sample, the chromatographic separation was obtained by an Acuity UHPLC CSH Phenyl-Hexyl column (1.7 μm, 2.1 × 150 mm) (Waters, US) with a guard column (Waters, US) with the same phase. The chromatographic and mass spectrometric condition is the same described by (Piai et al., 2019). Data were collected in a full scan from 65 to 900 Da in positive and from 65 to 450 Da in negative modes for further analysis. The data analysis was done with Compound Discoverer (CD) v. 3.1 (Thermo Scientific, USA).

2.5. Data analysis

2.5.1. Performance evaluation

To evaluate EO process performance, benzotriazole degradation efficiency (η_{BTA}), mineralization efficiency (η_{TOC}), and energy consumption (EC in kWh.g^{-1} benzotriazole) was followed and calculated according to the equations shown below Eq. (7-9) (Saha et al., 2020a).

$$\eta_{BTA} = \left(1 - \frac{c_f}{c_i}\right) \times 100\% \quad \text{(Eq.7)}$$

$$\eta_{TOC} = \left(1 - \frac{TOC_f}{TOC_i}\right) \times 100\% \quad \text{(Eq.8)}$$

$$EC = \frac{\sum_t V_t I_t \Delta t \times 10^{-3}}{m_f - m_i} \quad \text{(Eq.9)}$$

Where: c_i and c_f are the initial and final benzotriazole concentrations, respectively, in mg/L. TOC_i and TOC_f are the initial and final TOC concentrations, respectively, in mg/L. V_t is the cell voltage in V and I_t is the current at time t. Δt is the time interval in h. m_i and m_f are the initial and final benzotriazole masses, in g.

2.5.2. Synergistic effect

The synergistic effect of the electrolyte composition was evaluated by the synergy degree according to the equation Eq. (10), where, k_{ab} and k_a are benzotriazole removal rates constants, in min^{-1}, for mixed and individual salts, respectively (García-Espinoza et al., 2019). a is for sulfate and b is for chloride or nitrate.

$$S = \left(\frac{k_{ab} - k_a}{k_{ab}}\right) \times 100\% \quad \text{(Eq.10)}$$

2.5.3. Degradation by-products analysis

The raw LC-HRAM-MS data were processed by Compound Discoverer (CD) v. 3.1 (Thermo Scientific, USA). The COTPs were identified with the workflow template "Environmental w Stats Unknown ID w Online and Local Database Searches." The program used the differences between injected blanks and samples to select relevant peaks based on a minimum intensity (10^6 counts), mass tolerance (5 ppm), and retention time shift (0.2 min). The selected peaks were then assigned to the same compound with the same retention time (within the mentioned tolerance), the same measured mass (within the mentioned mass tolerance), matching the expected natural occurring isotope intensity, or the measured mass adducts formation. The extracted ion chromatogram (XIC) of these compounds was grouped together. The molecular formula was assigned according to the accurate mass and maximum element counts. The most matching compounds were selected from the ChemSpider database based on composition and mass lists. This resulted in a list of potential components evaluated by peak shape, peak area, and relevance to the parent compound.

3. Results and discussion

3.1. Effect of Na_2SO_4:$NaNO_3$ (SN) ratios on reactive sulfate species formation

The peroxydisulfate ($S_2O_8^{2-}$) formation rate at different Na_2SO_4:$NaNO_3$ (SN) ratios is presented in Fig. 2. In the 10:1 and 2:3 ratio, the $S_2O_8^{2-}$ formation rates are similar, around 60 μM/min, while the rate is only 17 μM/min in the 1:0 ratio (Fig. 2(a)). The low $S_2O_8^{2-}$ formation rate in the highest SN ratio (1:0) excludes pathways (a) and (b) from dominating. Besides, surface blocking by SO_4^{2-} hinders the $^{\bullet}OH$ formation, ultimately inhibiting the pathway (c). This blocking can be explained by the chemisorption phenomenon of SO_4^{2-} on the electrode surface. NO_3^- belonged to class IA adsorbates, which had coulombic attraction or solvent-structure breaking effects when binding to the surface (Anson, 2002). In contrast, SO_4^{2-} belonged to class IB adsorbates, which formed a covalent bond when attaching to the surface (Anson, 2002). Electrons were transferred from SO_4^{2-} to unoccupied orbitals to the electrode surface (Jia et al., 2015). Therefore, SO_4^{2-} has a stronger adsorption ability to the electrode than NO_3^-. Studies also show that the electro-oxidation rate constant of 2,4-DCP with BDD anode was low at high SO_4^{2-} concentration (0.9 h^{-1} in 0.3 M and 0.4 M Na_2SO_4) compared to the low SO_4^{2-} concentration (1.4 h^{-1} in 0.2 M Na_2SO_4) (Chen et al., 2018). This indicates that the high SO_4^{2-} concentration blocks the active radical formation, which decreases the rate constants.

The high $S_2O_8^{2-}$ formation rate in 10:1 and 2:3 ratios in Fig. 2(a) is noteworthy, increasing the possibility of the dominating pathway (c). According to Fig. 2(b), cyclic voltammetry shows that the water oxidation overpotential was around 1.74 V (vs. Ag/AgCl) in 1:0 ratio and shifted to 1.55 to 1.50 V (vs. Ag/AgCl) in the 10:1 and 1:10 ratios. The current density also increases sharply with the decreasing SO_4^{2-} ratio in the electrolyte, similar to the thiourea electrochemical oxidation study in sodium sulfate on a gold electrode, which shows that the current density decreased rapidly due to SO_4^{2-} chemisorbed (Jia et al., 2015). Thus, the mixing of salts can reduce surface blocking by SO_4^{2-} and increase the direct water oxidation to $^{\bullet}OH$ on the active sides of the BDD anode. The similar $S_2O_8^{2-}$ formation rates in 10:1 and 2:3 might be attributed to little influence of surface blocking by SO_4^{2-} and maximum $^{\bullet}OH$ formation. The 1:10 ratio has the lowest $S_2O_8^{2-}$ formation rate because of the lowest initial SO_4^{2-} concentration and $^{\bullet}OH$ scavenged by NO_3^-.

Moreover, the electrolyte's initial pH was 5.7. During the experiments, pH changed to 12.3 in 10:1 and 2:3 ratios, whereas 10.9 in 1:0 ratio (Fig. S1). SO_4^{2-} reaction with $^{\bullet}OH$ formed $SO_4^{\bullet-}$ and OH^- (Eq. (4)). The generation of OH^- contributes to the increase of pH.

These results indicate that increasing $^{\bullet}OH$ facilitates more $SO_4^{\bullet-}$ formation (Eqs. (4)–(6)), subsequently forming $S_2O_8^{2-}$. Thus, pathway (c) is more likely to be dominant, and $SO_4^{\bullet-}$ and $S_2O_8^{2-}$ formation can be boosted by mixing the SO_4^{2-} with IA anions like NO_3^- or Cl^- in a certain ratio range (10:1 to 2:3).

3.2. Effect of Na_2SO_4:$NaNO_3$ (SN) ratios on benzotriazole degradation

The electrochemical oxidation of benzotriazole with BDD anode was performed with different SN ratios, and benzotriazole concentration changed with reaction time is shown in Fig. 3. The benzotriazole

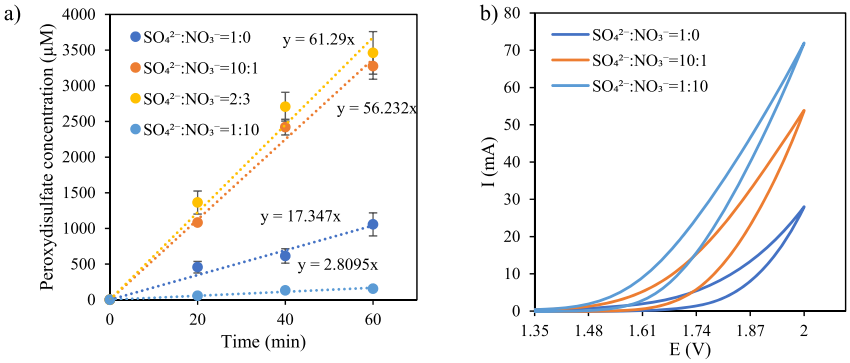

Fig. 2. (a) Peroxydisulfate concentration (μM) changing with reaction time (min) in different Na_2SO_4:$NaNO_3$ ratios. Experimental conditions: T = 25–30 °C, applied potential = 4.3 V (vs. Ag/AgCl), conductivity = 10 mS/cm, flow rate = 580 mL/min **(b)** cyclic voltammetry tests in different Na_2SO_4:$NaNO_3$ ratios; scan rate 50 mV/s, applied potential 0-2-0 (vs. Ag/AgCl), conductivity 10 mS/cm.

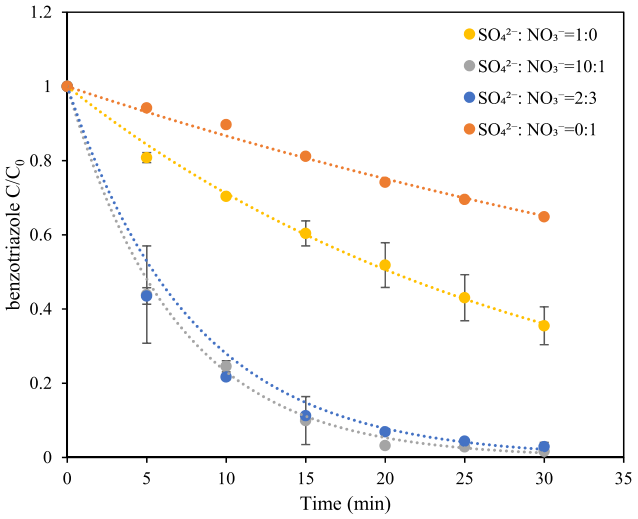

Fig. 3. Benzotriazole concentration changing with reaction time (min) in different Na_2SO_4:$NaNO_3$ (SN) ratios. Experimental conditions: 10 mg/L benzotriazole, different electrolyte ratios, T = 25–30 °C, applied potential = 4.3 V (vs. Ag/AgCl), conductivity = 10 mS/cm, flow rate = 580 mL/min.

removal was assumed to be a first-order reaction except in 0:1 ratio, and the rate constants in different ratios are given in Table 2.

The benzotriazole degradation rate reached 0.15 min^{-1} and 0.13 min^{-1} in 10:1 and 2:3 ratios, respectively. Like maximum $S_2O_8^{2-}$ formation, the faster benzotriazole degradation rate in 10:1 and 2:3 SN ratios can be explained by less SO_4^{2-} accumulation on the anode surface and more $^{\bullet}OH$, $SO_4^{\bullet-}$, and $S_2O_8^{2-}$ formation described in the previous section (3.1). Moreover, the benzotriazole degradation in 1:0 ratio was higher than in the 0:1 ratio (Fig. 2). In the 1:0 ratio, $^{\bullet}OH$, $SO_4^{\bullet-}$ and $S_2O_8^{2-}$ participated in benzotriazole degradation, whereas $^{\bullet}OH$ was the only dominating reactive oxidant in 0:1 ratio. Besides, the scavenging role of NO_3^- can also explain the benzotriazole degradation inhibition in 0:1 ratio. Experiments showed that humic acid removal efficiency by electron beam irradiation was reduced from 50% (no NO_3^-) to around 15% (100 mg/L NO_3^-) due to $^{\bullet}OH$ scavenging by NO_3^- (Ghaneian et al., 2013). Another literature also reported that NO_3^- interfered with the degradation pathway and scavenged $^{\bullet}OH$ during electrochemical degradation of diuron in a microreactor (Khongthon and Pavarajarn, 2016).

Furthermore, the initial pH changed from 6.9 to 9.6 in 1:0, 4.6 in 0:1, and 12.3 in 10:1 and 2:3 ratios (Fig. S3). This pH change indicates that the reaction of SO_4^{2-} with $^{\bullet}OH$ generates $SO_4^{\bullet-}$ and OH^- in 1:0, 10:1, and 2:3 SN ratios but was absent in an electrolyte with a 0:1 SN ratio (Eq. (4)). In addition, benzotriazole (pKa2 = 8.27) tends to lose one proton under the alkaline condition (Chen et al., 2018). This change of the benzotriazole molecular structure increases the electron density of the benzene ring, making it more accessible for oxidation by $SO_4^{\bullet-}$ (Chen et al., 2018; Ma et al., 2017, 2021). This explains why the benzotriazole degradation rate was the highest in 10:1 and 2:3 SN ratios.

The highest degree of synergy (57%) and mineralization efficiency (71%) was found in ratio 10:1 (Table 2). The energy consumption (0.43 kWh/g benzotriazole) was also the lowest in this ratio (Table 2). This result demonstrates that the 10:1 to 2:3 SN ratio was an optimum range to maximize the synergistic effect for reactive species formation.

Table 2
Comparison of benzotriazole degradation rate constant, degree of synergy, TOC removal efficiency and energy consumption in different Na_2SO_4:$NaNO_3$ (SN) ratios. Experimental conditions: 10 mg/L benzotriazole, T = 25–30 °C, applied potential = 4.3 V (vs. Ag/AgCl), conductivity = 10 mS/cm, flow rate = 580 mL/min reaction time = 30 min for rate constant, degree of synergy, energy consumption calculation and 60 min for TOC removal efficiency calculation.

SN ratio Na_2SO_4: $NaNO_3$	Chemical kinetic constant k (min^{-1})	Degree of synergy S (%)	TOC removal efficiency η_{TOC} (%) (±SD)	Energy consumption EC (kWh/g benzotriazole) (±SD)
1:0	0.034	–	56 (3)	0.82 (0.3)
10:1	0.15	77	71 (1)	0.43 (0.01)
2:3	0.13	74	62 (7)	0.58 (0.1)
0:1	–	–	52 (2)	1.78 (0.01)

3.3. Effect of Na_2SO_4:NaCl (SCl) ratios on benzotriazole degradation

The electrochemical oxidation of benzotriazole was also studied in different SCl ratios with BDD anodes. Benzotriazole concentration changed with reaction time is shown in Fig. 4. Same as section 3.2, it is assumed that the reactions were first-order excluding in 0:1 ratio, and the rate constants in different SCl ratios are listed in Table 3.

Like in the SN electrolyte, the 10:1 SCl ratio also has the highest benzotriazole degradation rate. In SCl electrolyte, the degradation rate in the 10:1 ratio reached 0.34 min^{-1}, ten times faster than in the 1:0 SCl ratio and faster than in the 0:1 SCl ratio (Fig. S4). It agrees with the investigation in sections 3.1 and 3.2. The addition of Cl^-, IA anion like NO_3^-reduces the excess surface blocking by chemisorption of SO_4^{2-} on the electrode. Which promotes the $^{\bullet}OH$ and subsequent $SO_4^{\bullet-}$ formation (pathway c). The initial pH changed from 6.9 to 9.6–9.9 in 1:0, 2:3, 0:1 ratios and 12.0 in 10:1 ratio (Fig. S5). A similar reason has been explained in section (3.2). It is worth mentioning that the benzotriazole degradation rate was two times faster in the 10:1 SCl ratio than in the 10:1 SN ratio (Fig. S2). The high reaction rate in the 10:1 SCl ratio can be explained by $Cl^{\bullet}$, and free chlorine mediated oxidation together with $^{\bullet}OH$, $SO_4^{\bullet-}$ and $S_2O_8^{2-}$ mediated oxidation. Other experiments also reported that Cl^- accelerated the perfluorooctanesulfonate degradation with BDD anode due to the active chlorine species formation (Wang et al., 2020).

However, the benzotriazole degradation rate decreases with the increase of the Cl^- ratio in the electrolyte. The $SO_4^{\bullet-}$ is scavenged by Cl^- to generate $Cl^{\bullet}$ and continue to react with Cl^- to generate fewer active radicals $Cl_2^{\bullet-}$ according to Eq. (11-12) (Stefan, 2017; Farhat et al., 2017; Ma et al., 2021). Previous research on resorcinol removal by EO with BDD anodes found that in Na_2SO_4 electrolyte, the rate constant decreased from 2.4 ± 0.18 h^{-1} to 0.51 ± 0.05 h^{-1} when Cl^- increased

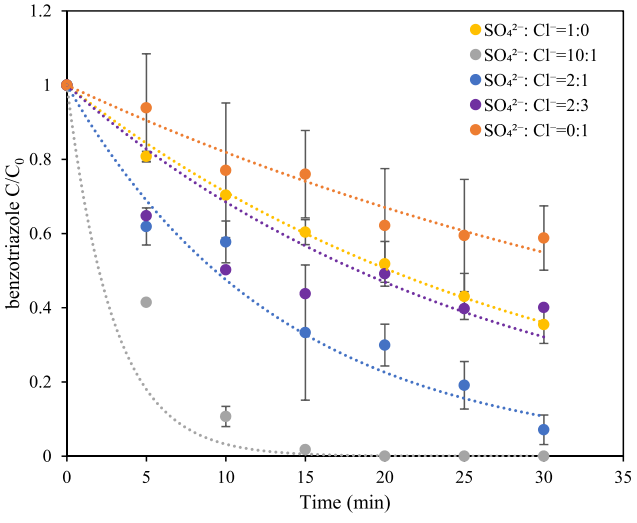

Fig. 4. Benzotriazole concentration changing with reaction time (min) in different Na_2SO_4:NaCl (SCl) ratios. Experimental conditions: 10 mg/L benzotriazole, T = 25–30 °C, applied potential = 4.3 V (vs. Ag/AgCl), conductivity = 10 mS/cm, flow rate = 580 mL/min.

Table 3
Comparison of benzotriazole degradation rate constant, degree of synergy, TOC removal efficiency and energy consumption in different Na_2SO_4:NaCl(SCl) ratios. Experimental conditions: 10 mg/L benzotriazole, T = 25–30 °C, applied potential = 4.3 V (vs. Ag/AgCl), conductivity = 10 mS/cm, flow rate = 580 mL/min, reaction time = 30 min for rate constant, degree of synergy, energy consumption calculation and 60 min for TOC removal efficiency calculation.

SCl ratio Na_2SO_4: NaCl	Chemical kinetic constant k (min^{-1})	Degree of synergy S (%)	TOC removal efficiency η_{TOC} (%) (±SD)	Energy consumption EC (kWh/g benzotriazole) (±SD)
1:0	0.034	–	56 (3)	0.82 (0.3)
10:1	0.34	90	83 (1)	0.40 (0.1)
2:1	0.074	54	62 (0)	0.51 (0.1)
2:3	0.038	11	57 (5)	0.88 (0.2)
0:1	–	–	38 (3)	0.93 (0.6)

from 0 mM to 20 mM (Farhat et al., 2017). Another research also concluded that Cl^- had a more significant influence on the $SO_4^{\bullet-}$ oxidation than $^{\bullet}OH$ oxidation because of $SO_4^{\bullet-}$ scavenging by Cl^- according to Eq. (11-12) (Yang et al., 2014).

$$SO_4^{\bullet-} + Cl^- \rightarrow SO_4^{2-} + Cl^{\bullet},\ k = 3.1 \times 10^8\ M^{-1}s^{-1} \quad \text{(Eq.11)}$$

$$Cl^{\bullet} + Cl^- \leftrightarrow Cl_2^{\bullet-},\ k = 1.4 \pm 0.2 \times 10^5\ M^{-1} \quad \text{(Eq.12)}$$

Same as in SN, the highest synergy degree (92%), benzotriazole mineralization efficiency (83%), and lowest energy consumption (0.40 kWh/g benzotriazole) are in the 10:1 SCl ratio (Table 3). So, there is a trend that the sulfate-rich ratios improve pollutants' degradation and decrease energy consumption.

3.4. Effect of Na_2SO_4:NaCl (SCl) ratios on chlorine by-product distribution during benzotriazole degradation

Chlorinated by-products formation, as free chlorine, chlorate (ClO_3-), perchlorate (ClO_4^-), and COTPs as AOX, were monitored during benzotriazole degradation in different SCl ratios. As shown in Fig. 5 (a), the free chlorine concentration in the 10:1 ratio becomes almost constant, while in 2:1, 2:3, and 0:1 ratio, the concentration continues to increase with time. The reaction of fresh free chlorine with $^{\bullet}OH$ to form ClO_3^- in 10:1 ratio kept the free chlorine concentration constant. According to Fig. 5 (a and b), the free chlorine concentration increases with initial chlorine ratios. Free chlorine is considered one of the precursors of AOX formation. Thus, the AOX concentration also increases with the free chlorine concentration in different ratios (Fig. 5(b)).

Fig. 5 (b) also shows that the ClO_3^- (134 mg/L) and ClO_4^- (156 mg/L) concentration was relatively higher in ratio 10:1 concerning initial Cl^- concentration (210 mg/L) (Fig. S6). According to the dominant pathway mentioned in section 3.1, more $^{\bullet}OH$ generation in SCl ratio 10:1, leading to complete conversion of free chlorine to ClO_3^-, which subsequently transformed to ClO_4^-. The ClO_3^- concentration jumped three times with increasing Cl^- ratio from 10:1 to 2:1 and decreased from 380 mg/L to 289 mg/L with further increasing Cl^- ratio from 2:1 to 0:1. Whereas ClO_4^- concentration decreased from 156 mg/L to 68 mg/L with an increasing Cl^- ratio from 10:1 to 0:1. The ClO_3^- and ClO_4^- formation mechanisms can explain their irregular concentration trend.

Free chlorine converted to ClO_3^- both non-radically and radically (Eq. 13–14) (Lan et al., 2017). By contrast, ClO_4^- is mainly generated radically from $^{\bullet}ClO_3$ and $^{\bullet}OH$. ClO_3^- is first chemisorbed on the BDD anode as $^{\bullet}ClO_3$ by directly one-electron transfer and then reacted with $^{\bullet}OH$ to produce ClO_4^- (Eq. (15-16)) (Lan et al., 2017; Farhat et al., 2017; Wang et al., 2020; Azizi et al., 2011; Brito et al., 2015; Donaghue and Chaplin, 2013). Due to both non-radically and radically free chlorine conversion, ClO_3^- formation jumped in the 2:1 SCl ratio solution. But because of less $^{\bullet}OH$ in 2:3 to 0:1 SCl ratio, ClO_3^- formation decreased. Besides, there was less available $^{\bullet}OH$ to participate in ClO_3^- to ClO_4^- conversion in 2:1, 2:3, and 0:1 ratio. Thus, a large amount of ClO_3^- was accumulated, and less ClO_4^- was generated in these ratios. ClO_3^- and ClO_4^- are harmful to the ecosystem, which is always a drawback of EO. Therefore, further research is necessary to minimize the toxic ClO_3^- and ClO_4^- formation.

$$6OCl^- + 3H_2O \rightarrow 2ClO_3^- + 4Cl^- + 6H^+ + 1.5O_2 + 6e^- \quad \text{(Eq.13)}$$

$$ClO^- \xrightarrow{\bullet OH} ClO_2^- \xrightarrow{\bullet OH} ClO_3 \quad \text{(Eq.14)}$$

$$ClO_3^- \rightarrow \bullet ClO_3 + e^- \quad \text{(Eq.15)}$$

$$\bullet ClO_3 + \bullet OH \rightarrow ClO_4^- + H^+ \quad \text{(Eq.16)}$$

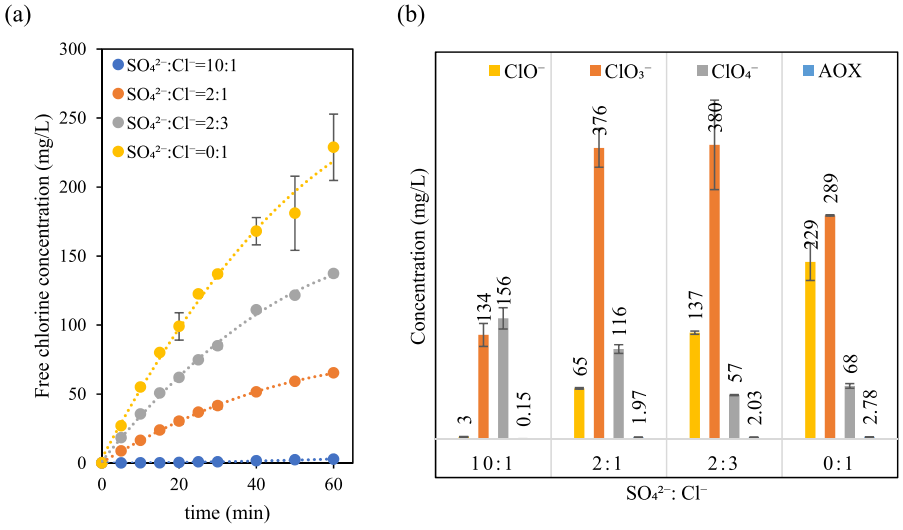

Fig. 5. (a) Free chlorine concentration changing with reaction time (min); (b) Free chlorine, chlorate, perchlorate and AOX concentration in different Na_2SO_4:NaCl (SCl) ratios after 60 min of treatment. Experimental conditions: 10 mg/L benzotriazole, T = 25–30 °C, applied potential = 4.3 V (vs. Ag/AgCl), conductivity = 10 mS/cm, flow rate = 580 mL/min, reaction time = 60 min.

3.5. Effect of Na_2SO_4:NaCl (SCl) ratios on transformation products distribution during benzotriazole degradation

Seven chlorinated organic transformation products (COTPs), COTP-1 ($C_6H_4ClN_3$), COTP-2 ($C_6H_3Cl_2N_3$), COTP-3 (C_4H_6ClNO), COTP-4 ($C_2H_2Cl_2O_2$), COTP-5($C_2HCl_2N_3$), COTP-6 ($C_5HCl_3O_3$), and COTP-7 ($C_3H_2Cl_2N_2$), were detected during the EO of benzotriazole (Table 4). COTP-1 represents the chlorination on the benzene ring. Active chlorine species are capable of electrophilic substitution in C4 and C7 positions on the benzene ring (Yang et al., 2021). Thus, two chromatographic peaks corresponding to 153.00966 m/z at 8.445- and 8.807-min retention time represent two isomers of COTP-1 (Table 4 and Fig. S7). The active chlorine species could further chlorinate COTP-1 to produce COTP-2. In 0:1 ratio, COTP-1 and COTP-2 were found. In the 0:1 ratio, more active chlorine species were formed (Fig. 5), and the benzotriazole degradation rate was low (0.02 min^{1}). Thus, benzotriazole was exposed to active chlorine species for a longer time, enhancing these two COTPs. Two similar COTPs are detached during the chlorination of benzotriazole (Yang et al., 2021), xylyltriazole (XTRi), and 2-amino-benzothiazole (Nika et al., 2017). In the 2:3 ratio, only COTP-1 was detected. This can be explained by the steric effect and the extent of exposure to active chlorine species. When one chlorine atom is added to the benzene ring, it will be difficult for another chlorine atom to be added on (Stefan, 2017). During EO of 4-ethylphenol in chloride electrolyte, 2-chloro-4-ethylphenol (2C4EP) was detected earlier than 2, 6-dichloro-4-ethylphenol (26DC4EP). Besides, 2C4EP and 26DC4EP formation were faster at high than at low Cl^- concentrations (Bruninghoff et al., 2019). Thus, this reduces the possibilities for COTP-2 formation in lower SCl ratios. In 2:1 ratio, most of the benzotriazole was oxidized quickly (rate constant = 0.074 min^{-1}) and was not exposed to active chlorine species; therefore, none of these two COTPs were observed under these conditions.

Oxidation of organic compounds produces carbonaceous and nitrogenous intermediates before being mineralized to carbon dioxides. These intermediates react with active chlorine species to form COTPs (Yang et al., 2021). Initially, oxidation and radicles attack the C6 position on the benzene ring to open the ring to produce carbonaceous intermediates like TP-1. TP-1 further goes through hydroxylation, bond cleaving, and chlorination to make COPT-4 and COPT-5. On the other hand, Nitrogenous intermediates were produced through the opening of the triazole ring. Which further oxidize, break down, and are chlorinated to form COTP-3 and COTP-7. These COTPs were detected in 2:1, 2:3, and 0:1 SCl ratios. However, none of the chlorinated intermediate compounds were seen in the solution with a 10:1 SCl ratio. Free chlorine concentrations were too low and were quickly converted to chlorate and perchlorate in the 10:1 SCl ratio solution. Also, faster simultaneous $^{\bullet}OH$ and $SO_4^{\bullet-}$ formation in 10:1 SCl ratio facilitated more rapid degradation of benzotriazole and its intermediates. Moreover, $^{\bullet}OH$ radicals, indeed, manly react to initiate substitution, cleavage of C=C bond, and oxidation of the benzene ring. These $SO_4^{\bullet-}$ radicals are, on the other hand, more inclined to attack the conjugation bond in the molecules (Li et al., 2020). However, a small amount of AOX was still detected in the 10:1 SCl ratio solution (Fig. 5). Some small amounts of COTPs formed, which could not be identified in the used LC-MS analysis. In a nutshell, sulfate-rich electrolytes could significantly minimize the formation of chlorinated organic transformation products (COTPs).

3.6. Environmental implications

In practice, many industrial wastewater effluents, landfill leachates, and municipal wastewater contain dissolved salts and POPs (Bagastyo et al., 2020; Linaric et al., 2013; Pernetti and Di Palma, 2005; Lefebvre and Moletta, 2006; Koeman-Stein et al., 2016; Saha et al., 2020b; Foglia et al., 2020). This study shows that the dissolved salts in wastewater effluents can be beneficial as well as detrimental for EO removal of organic bio recalcitrant organic pollutants. It was also found that the electrolyte composition plays an important role in organic compounds degradation, mineralization, energy consumption, and chlorinated byproduct formation. Therefore, regulating the concentration of dissolved salts is essential for EO's successful and environmentally safe

Table 4
List of chlorinated organic transformation products (COTPs) and non-chlorinated transformation products (TPs) detected during benzotriazole degradation in different Na_2SO_4:NaCl (SCl).

COTPs	Propose Formula	Propose structure	Molecular weight (m/z)	Accuracy (ppm)	Retention Time (min)	Mode (positive/ negative)	Na_2SO_4:NaCl (SCl) ratios				
							1:0	10:1	2:1	2:3	0:1
COTP-1	$C_6H_4ClN_3$	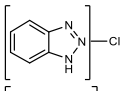	153.00966	1.89	8.445 8.807	+	ND	ND	ND	✓	✓
COTP-2	$C_6H_3Cl_2N_3$	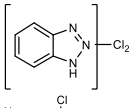	186.97071	1.63	9.485 9.694	+	ND	ND	ND	ND	✓
COTP-3	C_4H_6ClNO		119.01407	2.31	6.177	+	ND	ND	✓	✓	✓
COTP-4	$C_2H_2Cl_2O_2$		127.94306	−0.94	8.694	–	ND	ND	✓	✓	✓
COTP-5	$C_2HCl_2N_3$		136.9546	−1.15	9.256	–	ND	ND	✓	✓	✓
COTP-6	$C_5HCl_3O_3$	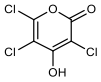	213.89919	0.22	15.14	–	ND	ND	✓	✓	✓
COTP-7	$C_3H_2Cl_2N_2$		135.95981	2.25	8.134	+	ND	ND	✓	ND	✓
non-chlorinated transformation products (TPs)											
TP-1	$C_4H_3N_3O_4$	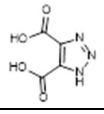	157.01269	−3.02	9.153	–	ND	✓	✓	✓	✓

application. Nanofiltration is an attractive accompanying technology for controlling the SN and SCl ratios between 10:1 and 2:1 in the effluents treated with EO. In these ratios, electrochemical oxidation has a high degradation rate, high mineralization efficiency, and low energy consumption due to effective $^{\bullet}OH$ and reactive $SO_4^{\bullet-}$ and $S_2O_8^{2-}$ formation discussed in sections 3.1-3.3. Low Cl^- concentration will also decrease the COTPs formation addressed in sections 3.3 and 3.4. Therefore, electrochemical oxidation combined with nanofiltration is a promising combination and worthy of further investigation.

4. Conclusions

The influence of electrolyte composition on the active sulfate formation and chlorinated by-product distribution in electrochemical degradation of benzotriazole with boron-doped diamond (BDD) anode has been investigated in this research. First, the study shows that $SO_4^{\bullet-}$ has been formed dominantly via $^{\bullet}OH$ on the electrode surface. Active sulfate species formation was faster in sulfate-rich SN ratios. In contrast, in 1:0 ratio, excess SO_4^{2-}chemisorbs on the BDD anode and hampers the active sulfate species formation. Thereby, the 10:1 SN and SCl ratio have the highest benzotriazole degradation rate, mineralization efficiency, synergistic degree, and lowest energy consumption. Decreasing concentrations of Cl^- in SCl solutions leads to less toxic chlorinated organic transformation products and active chlorine formation. LC-MS has analyzed none of the chlorinated organic transformation products in the SCl 10:1 ratio, which -in contrast-were found in all other chloride enriched ratios above this value. However, chlorate and perchlorate concentrations were comparatively higher in the 10:1 ratio due to $^{\bullet}OH$ generation. Nanofiltration could lead to a sulfate-rich concentrate suitable for electrochemical oxidation in an actual application. Thus, it is promising to combine electrochemical oxidation with nanofiltration, however, the economic and environmental feasibility of the combination still needs further research. In addition, to ger more insides, it is recommended to compare other in-between ratios such as 3:2.

Funding sources

This research is financed by the Netherlands Organisation for Scientific Research (NWO), which is partly funded by the Ministry of Economic Affairs and Climate Policy and co-financed by the Netherlands Ministry of Infrastructure and Water Management and partners of the Dutch Water Nexus consortium (project number 14301).

Declaration of competing interest

The authors declare that they have no known competing financial interests or personal relationships that could have appeared to influence the work reported in this paper.

Acknowledgments

This research is financed by the Netherlands Organisation for Scientific Research (NWO), which is partly funded by the Ministry of Economic Affairs and Climate Policy and co-financed by the Netherlands Ministry of Infrastructure and Water Management and partners of the Dutch Water Nexus consortium (project number 14301). Especially Magneto special anodes BV and is acknowledged for providing the electrodes.

Appendix A. Supplementary data

Supplementary data to this article can be found online at https://doi.org/10.1016/j.envres.2022.113057.

References

Anson, F.C., 2002. Patterns of ionic and molecular adsorption at electrodes. Acc. Chem. Res. 8, 400–407.
Araújo, K.C. de F., Barreto, J.P. de P., Cardozo, J.C., dos Santos, E.V., de Araújo, D.M., Martínez-Huitle, C.A., 2018. Sulfate pollution: evidence for electrochemical production of persulfate by oxidizing sulfate released by the surfactant sodium dodecyl sulfate. Environ. Chem. Lett. 16, 647–652.
Azizi, O., Hubler, D., Schrader, G., Farrell, J., Chaplin, B.P., 2011. Mechanism of perchlorate formation on boron-doped diamond film anodes. Environ. Sci. Technol. 45, 10582–10590.
Bagastyo, A.Y., Novitasari, D., Nurhayati, E., Direstiyani, L.C., 2020. Impact of sulfate ion addition on electrochemical oxidation of anaerobically treated landfill leachate using boron-doped diamond anode. Res. Chem. Intermed. 46, 4869–4881.
Brillas, E., 2021. Recent development of electrochemical advanced oxidation of herbicides. A review on its application to wastewater treatment and soil remediation. J. Clean. Prod. 290.
Brito, C.d.N., de Araújo, D.M., Martínez-Huitle, C.A., Rodrigo, M.A., 2015. Understanding active chlorine species production using boron doped diamond films with lower and higher sp3/sp2 ratio. Electrochem. Commun. 55, 34–38.
Bruguera-Casamada, C., Sires, I., Prieto, M.J., Brillas, E., Araujo, R.M., 2016. The ability of electrochemical oxidation with a BDD anode to inactivate Gram-negative and Gram-positive bacteria in low conductivity sulfate medium. Chemosphere 163, 516–524.
Bruninghoff, R., van Duijne, A.K., Braakhuis, L., Saha, P., Jeremiasse, A.W., Mei, B., Mul, G., 2019. Comparative analysis of photocatalytic and electrochemical degradation of 4-ethylphenol in saline conditions. Environ. Sci. Technol. 53, 8725–8735.
Burgos-Castillo, R.C., Sires, I., Sillanpaa, M., Brillas, E., 2018. Application of electrochemical advanced oxidation to bisphenol A degradation in water. Effect of sulfate and chloride ions. Chemosphere 194, 812–820.
Chen, L., Lei, C., Li, Z., Yang, B., Zhang, X., Lei, L., 2018. Electrochemical activation of sulfate by BDD anode in basic medium for efficient removal of organic pollutants. Chemosphere 210, 516–523.
Clematis, D., Panizza, M., 2021. Electrochemical oxidation of organic pollutants in low conductive solutions. Current Opinion in Electrochemistry 26.
da Costa, T., Santos, J., da Silva, D., Martinez-Huitle, C., 2019. BDD-electrolysis of oxalic acid in diluted acidic solutions. J. Braz. Chem. Soc. 30, 1541–1547.
Davis, J., Baygents, J.C., Farrell, J., 2014. Understanding persulfate production at boron doped diamond film anodes. Electrochim. Acta 150, 68–74.
Devi, L.G., Munikrishnappa, C., Nagaraj, B., Rajashekhar, K.E., 2013. Effect of chloride and sulfate ions on the advanced photo Fenton and modified photo Fenton degradation process of Alizarin Red S. J. Mol. Catal. Chem. 374, 125–131.
Donaghue, A., Chaplin, B.P., 2013. Effect of select organic compounds on perchlorate formation at boron-doped diamond film anodes. Environ. Sci. Technol. 47, 12391–12399.
dos Santos, A.J., Kronka, M.S., Fortunato, G.V., Lanza, M.R.V., 2021. Recent advances in electrochemical water technologies for the treatment of antibiotics: a short review. Current Opinion in Electrochemistry 26.
Farhat, A., Keller, J., Tait, S., Radjenovic, J., 2015. Removal of persistent organic contaminants by electrochemically activated sulfate. Environ. Sci. Technol. 49, 14326–14333.
Farhat, A., Keller, J., Tait, S., Radjenovic, J., 2017. Assessment of the impact of chloride on the formation of chlorinated by-products in the presence and absence of electrochemically activated sulfate. Chem. Eng. J. 330, 1265–1271.
Foglia, A., Akyol, C., Frison, N., Katsou, E., Eusebi, A.L., Fatone, F., 2020. Long-term operation of a pilot-scale anaerobic membrane bioreactor (AnMBR) treating high salinity low loaded municipal wastewater in real environment. Separ. Purif. Technol. 236.
Ganiyu, S.O., Martínez-Huitle, C.A., Oturan, M.A., 2021. Electrochemical advanced oxidation processes for wastewater treatment: advances in formation and detection of reactive species and mechanisms. Current Opinion in Electrochemistry 27.
García-Espinoza, J.D., Zolfaghari, M., Mijaylova Nacheva, P., 2019. Synergistic effect between ultraviolet irradiation and electrochemical oxidation for removal of humic acids and pharmaceuticals. Water Environ. J. 34, 232–246.
Ghaneian, M.T., Ehrampoush, M.H., Jasemizad, T., Kheirkha, M., Amraei, R., Sahlabadi, F., 2013. The effect of nitrate as a radical scavenger for the removal of humic acid from aqueous solutions by electron beam irradiation. Journal of Community Health Research 1, 134–143.
Gokulakrishnan, S., Mohammed, A., Prakash, H., 2016. Determination of persulphates using N,N-diethyl-p-phenylenediamine as colorimetric reagent: oxidative coloration and degradation of the reagent without bactericidal effect in water. Chem. Eng. J. 286, 223–231.
Grebel, J.E., Pignatello, J.J., Mitch, W.A., 2010. Effect of halide ions and carbonates on organic contaminant degradation by hydroxyl radical-based advanced oxidation processes in saline waters. Environ. Sci. Technol. 44, 6822–6828.
Groenen Serrano, K., 2018. Indirect electrochemical oxidation using hydroxyl radical, active chlorine, and peroxodisulfate. In: Electrochemical Water and Wastewater Treatment, pp. 133–164.
Hu, Z., Cai, J., Song, G., Tian, Y., Zhou, M., 2021. Anodic oxidation of organic pollutants: anode fabrication, process hybrid and environmental applications. Current Opinion in Electrochemistry 26.
Jia, Y., Zhao, Y., He, Y., Pan, C., Ji, C., Bi, W., Gao, Q., 2015. Chemisorbed sulfate-driven oscillatory electro-oxidation of thiourea on gold. J. Phys. Chem. C 119, 24837–24843.

Jin, Y., Cho, K., Chung, C.M., Hong, S., 2020. Sulfate ion removal from reverse osmosis concentrate using electrodialysis and nano-filtration in combination with ettringite precipitation. In: Frontiers in Water-Energy-Nexus—Nature-Based Solutions, Advanced Technologies and Best Practices for Environmental Sustainability, pp. 407–410.

Khongthon, W., Pavarajarn, V., 2016. Effect of nitrate and sulfate contamination on degradation of diuron via electrochemical advanced oxidation in a microreactor. Eng J-Thail 20, 25–34.

Koeman-Stein, N.E., Creusen, R.J.M., Zijlstra, M., Groot, C.K., van den Broek, W.B.P., 2016. Membrane distillation of industrial cooling tower blowdown water. Water Resources and Industry 14, 11–17.

Lan, Y., Coetsier, C., Causserand, C., Groenen Serrano, K., 2017. On the role of salts for the treatment of wastewaters containing pharmaceuticals by electrochemical oxidation using a boron doped diamond anode. Electrochim. Acta 231, 309–318.

Lefebvre, O., Moletta, R., 2006. Treatment of organic pollution in industrial saline wastewater: a literature review. Water Res. 40, 3671–3682.

Li, X., Zhang, D., Liu, Z., Lyu, C., Niu, S., Dong, Z., Lyu, C., 2020. Enhanced catalytic oxidation of benzotriazole via peroxymonosulfate activated by CoFe2O4 supported onto nitrogen-doped three-dimensional graphene aerogels. Chem. Eng. J. 400.

Linaric, M., Markic, M., Sipos, L., 2013. High salinity wastewater treatment. Water Sci. Technol. 68, 1400–1405.

Ma, J., Li, H., Chi, L., Chen, H., Chen, C., 2017. Changes in activation energy and kinetics of heat-activated persulfate oxidation of phenol in response to changes in pH and temperature. Chemosphere 189, 86–93.

Ma, J., Ding, Y., Chi, L., Yang, X., Zhong, Y., Wang, Z., Shi, Q., 2021. Degradation of benzotriazole by sulfate radical-based advanced oxidation process. Environ. Technol. 42, 238–247.

Martinez-Huitle, C.A., Rodrigo, M.A., Sires, I., Scialdone, O., 2015. Single and coupled electrochemical processes and reactors for the abatement of organic water pollutants: a critical review. Chem. Rev. 115, 13362–13407.

Nika, M.C., Bletsou, A.A., Koumaki, E., Noutsopoulos, C., Mamais, D., Stasinakis, A.S., Thomaidis, N.S., 2017. Chlorination of benzothiazoles and benzotriazoles and transformation products identification by LC-HR-MS/MS. J. Hazard Mater. 323, 400–413.

Panizza, M., Cerisola, G., 2009. Direct and mediated anodic oxidation of organic pollutants. Chem. Rev. 109, 6541–6569.

Pernetti, M., Di Palma, L., 2005. Experimental evaluation of inhibition effects of saline wastewater on activated sludge. Environ. Technol. 26, 695–703.

Piai, L., Dykstra, J.E., Adishakti, M.G., Blokland, M., Langenhoff, A.A.M., van der Wal, A., 2019. Diffusion of hydrophilic organic micropollutants in granular activated carbon with different pore sizes. Water Res. 162, 518–527.

Saha, P., Bruning, H., Wagner, T.V., Rijnaarts, H.H.M., 2020a. Removal of organic compounds from cooling tower blowdown by electrochemical oxidation: role of electrodes and operational parameters. Chemosphere 259, 127491.

Saha, P., Wagner, T.V., Ni, J., Langenhoff, A.A.M., Bruning, H., Rijnaarts, H.H.M., 2020b. Cooling tower water treatment using a combination of electrochemical oxidation and constructed wetlands. Process Saf. Environ. Protect. 144, 42–51.

Saha, P., Wang, Y., Moradi, M., Brüninghoff, R., Moussavi, G., Mei, B., Mul, G., Rijnaarts, H.H.M., Bruning, H., 2021. Advanced Oxidation Processes for Removal of Organics from Cooling Tower Blowdown: Efficiencies and Evaluation of Chlorinated Species. Separation and Purification Technology.

Salazar-Banda, G.R., Santos, G.d.O.S., Duarte Gonzaga, I.M., Dória, A.R., Barrios Eguiluz, K.I., 2021. Developments in electrode materials for wastewater treatment. Current Opinion in Electrochemistry 26.

Santos, J.E.L., Antonio Quiroz, M., Cerro-Lopez, M., de Moura, D.C., Martínez-Huitle, C. A., 2018. Evidence for the electrochemical production of persulfate at TiO2 nanotubes decorated with PbO2. New J. Chem. 42, 5523–5531.

Santos, G.O.S., Eguiluz, K.I.B., Salazar-Banda, G.R., Saez, C., Rodrigo, M.A., 2020. Understanding the electrolytic generation of sulfate and chlorine oxidative species with different boron-doped diamond anodes. J. Electroanal. Chem. 857.

Seibert, D., Zorzo, C.F., Borba, F.H., de Souza, R.M., Quesada, H.B., Bergamasco, R., Baptista, A.T., Inticher, J.J., 2020. Occurrence, statutory guideline values and removal of contaminants of emerging concern by Electrochemical Advanced Oxidation Processes: a review. Sci. Total Environ. 748, 141527.

Serrano, K., Michaud, P.A., Comninellis, C., Savall, A., 2002. Electrochemical preparation of peroxodisulfuric acid using boron doped diamond thin film electrodes. Electrochim. Acta 48, 431–436.

Shin, Y.-U., Yoo, H.-Y., Ahn, Y.-Y., Kim, M.S., Lee, K., Yu, S., Lee, C., Cho, K., Kim, H.-i., Lee, J., 2019. Electrochemical oxidation of organics in sulfate solutions on boron-doped diamond electrode: multiple pathways for sulfate radical generation. Appl. Catal. B Environ. 254, 156–165.

Stefan, M.I., 2017. Advanced Oxidation Processes for Water Treatment: Fundamentals and Applications. IWA Publishing.

Thiam, A., Salazar, R., Brillas, E., Sirés, I., 2018. Electrochemical advanced oxidation of carbofuran in aqueous sulfate and/or chloride media using a flow cell with a RuO2-based anode and an air-diffusion cathode at pre-pilot scale. Chem. Eng. J. 335, 133–144.

Villegas-Guzman, P., Hofer, F., Silva-Agredo, J., Torres-Palma, R.A., 2017. Role of sulfate, chloride, and nitrate anions on the degradation of fluoroquinolone antibiotics by photoelectro-Fenton. Environ. Sci. Pollut. Control Ser. 24, 28175–28189.

Wang, L., Lu, J., Li, L., Wang, Y., Huang, Q., 2020. Effects of chloride on electrochemical degradation of perfluorooctanesulfonate by Magneli phase Ti4O7 and boron doped diamond anodes. Water Res. 170, 115254.

Yang, Y., 2020. Recent advances in the electrochemical oxidation water treatment: spotlight on byproduct control. Front. Environ. Sci. Eng. 14.

Yang, Y., Pignatello, J.J., Ma, J., Mitch, W.A., 2014. Comparison of halide impacts on the efficiency of contaminant degradation by sulfate and hydroxyl radical-based advanced oxidation processes (AOPs). Environ. Sci. Technol. 48, 2344–2351.

Yang, T., Mai, J., Wu, S., Liu, C., Tang, L., Mo, Z., Zhang, M., Guo, L., Liu, M., Ma, J., 2021. UV/chlorine process for degradation of benzothiazole and benzotriazole in water: efficiency, mechanism and toxicity evaluation. Sci. Total Environ. 760, 144304.

Zhang, C., He, Z., Wu, J., Fu, D., 2015. The peculiar roles of sulfate electrolytes in BDD anode cells. J. Electrochem. Soc. 162, E85–E89.